Linear polarization of the $2p^5 3s \rightarrow 2p^6$ lines following the inner-shell photoionization of sodiumlike ions

M. K. Inal*
LPT, Département de Physique, Université A. Belkaid, B.P. 119, 13000 Tlemcen, Algeria

A. Surzhykov and S. Fritzsche
Institut für Physik, Universität Kassel, Heinrich-Plett Strasse 40, D-34132 Kassel, Germany
(Received 8 August 2005; published 31 October 2005)

The inner-shell photoionization of highly charged, many-electron ions and their subsequent radiative decay are studied theoretically within the multiconfiguration Dirac-Fock approach. Special attention is paid to the linear polarization of the characteristic x-ray radiation. Detailed calculations have been carried out, in particular for the $2p^5 3s \rightarrow 2p^6$ radiative transitions following ionization of the $2p$ electron of the sodiumlike iron Fe^{15+} and uranium U^{81+} ions. For these elements, the inner-shell photoionization was found to induce the (relatively) low linear polarization of the subsequently emitted photons which is strongly affected, moreover, by the higher-order (nondipole) effects in the electron-photon interaction.

DOI: 10.1103/PhysRevA.72.042720 PACS number(s): 32.80.Fb, 32.50.+d, 32.30.Rj

I. INTRODUCTION

Both collisional excitation and inner-shell ionization of target ions by the beams of unpolarized electrons, protons, or photons may lead to an *alignment* of excited ionic states with respect to the incident beam direction [1–4]. Such an alignment—i.e., the unequal population of the ion sublevels with the different modulus of magnetic quantum number $|M_J|$—results later in the emission of decay x-ray photons which have an anisotropic angular distribution as well as a nonzero linear polarization [5,6]. This—fluorescence—polarization has been of long-term interest for both experiment and theory since it can be used as a precise tool for the diagnostic of the energy and angular distributions of nonthermal charged particles (electrons, protons, or ions) accelerated in high-temperature astrophysical and laboratory plasmas [7–10]. Moreover, the x-ray polarization studies are playing an important role in understanding the relativistic as well as the electron-electron interaction effects in energetic collisions of highly charged ions. To explore such effects, a number of x-ray polarization measurements have been performed recently at the electron beam ion trap (EBIT) facility at Lawrence Livermore National Laboratory [11–13] and were generally found in good agreement with calculations, based on the Dirac theory [6,14–17].

Until now, most of the experimental and theoretical studies of the x-ray polarization have dealt with the *electron-ion* collisions. Much less attention, in contrast, has been previously paid to the linear polarization of x-ray lines following the inner-shell *photoionization* of the highly charged ions. This inner-shell photoionization plays an important role, however, in optically thick and dense astrophysical plasmas exposed to strong x-ray emission from many astrophysical sources such as stellar flares, binary stars, supernova remnants, or accreting black holes [18]. Detailed information about such sources may be obtained by studying the linear polarization of characteristic x-ray photons as emitted from photoionized plasma clouds.

Beside astrophysical studies, new interest arises also to explore the inner-shell photoionization processes in *laboratory* plasmas. In particular, with the recent progress in ion trap techniques as well as in the setup of intensive light sources in the EUV and x-ray domain, such as fourth-generation synchrotron facilities or variously proposed free-electron lasers, experiments on the (photo)ionization of highly charged ions have now become more likely to be carried out in the future. With the increasing of the nuclear charge of the ions (and the incoming photon energies), such experiments may help to investigate the relativistic as well as the nondipole effects on the inner-shell vacancy production and linear polarization of the subsequently emitted photons.

In this contribution, the relativistic Dirac's theory is applied to analyze the linear polarization of characteristic x-ray photons following the inner-shell ionization of highly charged, medium-Z, and high-Z ions. Of course, such polarization studies require first knowledge of the magnetic sublevel population of the excited ion states as it arises from the photoionization process. Here we suppose that this population is completely defined by the partial cross sections for the (photo)ionization to particular magnetic sublevels. In Sec. II A, therefore, we will briefly discuss the evaluation of photoionization partial cross sections within the relativistic framework and by taking into account the full multipole decomposition for the electron-photon interaction operator. By utilizing these cross sections, in Sec. II B we will derive the polarization Stokes parameters for the x-ray photons as emitted in the radiative decay of the excited ion states. In Sec. III, these Stokes parameters are then calculated in the framework of the multiconfiguration Dirac-Fock (MCDF) method. Detailed computations have been carried out, in particular, for the magnetic quadrupole transition $2p^5 3s\ ^3P_2 \rightarrow 2p^6\ ^1S_0$ and two electric dipole transitions $2p^5 3s\ ^1P_1 \rightarrow 2p^6\ ^1S_0$ and $2p^5 3s\ ^3P_1 \rightarrow 2p^6\ ^1S_0$ following the photoionization of the $2p$

*Electronic address: m_inal@mail.univ-tlemcen.dz

 ©2005 The American Physical Society

electron of the (initially) sodiumlike iron Fe^{15+} and uranium U^{81+} ions. For these three lines, the polarization Stokes parameters are discussed in Sec. IV as a function of the incoming photon energy and compared with those from the electric-dipole approximation—i.e., obtained by including only the leading electric dipole term in the photoionization cross sections. As seen from our calculations, the linear polarization of the $2p^5 3s \rightarrow 2p^6$ characteristic photons does not exceed 10% and, moreover, alters if higher-multipole corrections are taken into account for the inner-shell photoionization. Finally, a brief summary and outlook are given in Sec. V.

II. THEORY

A. Photoionization cross sections to specific magnetic sublevels of the final ion

Not much has to be said about the basic formalism for studying the photoionization of the many-electron atoms (or ions). In the past, this formalism has been widely applied to explore not only the total ionization cross sections but also the angular distributions and even polarization of the emitted photoelectrons [19–25]. Usually, the analysis of these properties of the photoionization process can be traced back to the evaluation of the transitions amplitude

$$f(M_a, m_s, \lambda, M_0) = \left(\frac{4\pi^2\alpha}{\omega}\right)^{1/2} \times \left\langle \alpha_a J_a M_a, \boldsymbol{p} m_s \left| \sum_{i=1}^{N} \boldsymbol{\alpha}_i \mathbf{u}_\lambda e^{i\boldsymbol{k}\cdot\boldsymbol{r}_i} \right| \alpha_0 J_0 M_0 \right\rangle, \quad (1)$$

which describes the emission of the electron with asymptotic momentum $\boldsymbol{p}$ and spin projection m_s under the simultaneous absorption of the photon with the wave vector $\boldsymbol{k}$ and helicity $\lambda = \pm 1$. In this amplitude, moreover, the ion *before* and *after* photoionization is supposed to be in the states $|\alpha_0 J_0 M_0\rangle$ and $|\alpha_a J_a M_a\rangle$ with well-defined total angular momentum J, M owing to its symmetry and where α denotes all the additional quantum numbers as needed for a unique specification of the states.

As is seen from Eq. (1), the transition amplitude $f(M_a, m_s, \lambda, M_0)$ depends both on the spin projections of the incoming photon λ and the emitted electron m_s and on the magnetic quantum numbers M_0 and M_a of the initial and final ion states, respectively. However, while the photon helicity λ is *always* defined with respect to the direction of photon's propagation $\boldsymbol{k}$, the other spin projections are related to the *quantization axis* of the overall system (z axis). As discussed previously [26], the proper choice of this quantization axis and, hence, the projection above depends both on the particular process under consideration and on the geometry in which the experiments are carried out. For instance, to explore the alignment of the excited ion states following inner-shell ionization by *unpolarized* light, it is convenient to adopt the quantization axis along the incoming photon momentum: $\boldsymbol{k} \| z$. Such a choice of the quantization axis allows us to establish the *partial* cross sections for the photoionization to a specific magnetic state $|\alpha_a J_a M_a\rangle$ of the residual ion [4,19,20]:

$$\sigma(\alpha_0 J_0 \rightarrow \alpha_a J_a M_a, \epsilon) = \frac{1}{2(2J_0+1)} \sum_{M_0 \lambda m_s} \int d\Omega_p |f(M_a, m_s, \lambda, M_0)|^2, \quad (2)$$

where we assume that the ions in the initial states are unpolarized and that neither the emission angle of the photoelectrons nor their polarization states are observed.

Making use of Eqs. (1) and (2), the computation of the partial photoionization cross sections requires an integration over all directions $\hat{\mathbf{p}} = (\theta_p, \phi_p)$ of the emitted (photo) electron in 4π. As usual in atomic physics, such an integration can be easily performed by applying the *decomposition* of the free-electron wave function into its partial waves, an expansion which depends on the choice of the quantization axis. By adopting, for instance, the quantization axis along the incoming photon momentum, we have to carry out a rotation of the space part of the electron wave function from the z to the $\hat{p}$ direction [20,27]:

$$|\mathbf{p} m_s\rangle = \sum_{\kappa m_j} i^l e^{-i\Delta_\kappa} \langle l m_l 1/2 m_s | j m_j \rangle Y^*_{l m_l}(\hat{\mathbf{p}}) | \epsilon l j m_j \rangle, \quad (3)$$

where the summation runs over all partial waves $\kappa = \pm 1, \pm 2, \ldots$—i.e., over all possible values of the Dirac angular momentum quantum number $\kappa = \pm(j+1/2)$ for $l = j \pm 1/2$. In this notation, the (nonrelativistic angular) momentum l represents the parity of the partial waves and Δ_κ is the Coulomb phase shift [20,21].

To obtain now the partial-wave expansion of the *many-electron* scattering states in the transition amplitude (1), we combine Eq. (3) with the standard procedure for the coupling of two angular momenta:

$$|\alpha_a J_a M_a, \mathbf{p} m_s\rangle = \mathcal{A} \sum_{\kappa m_j} i^l e^{-i\Delta_\kappa} \langle l m_l 1/2 m_s | j m_j \rangle Y^*_{l m_l}(\hat{\mathbf{p}}) \times \sum_{JM} \langle J_a M_a j m_j | J M \rangle | (\alpha_a J_a, \epsilon l j) J M \rangle, \quad (4)$$

where the operator $\mathcal{A}$ is used to ensure a proper antisymmetrization of the emitted photoelectron with respect to the bound-state wave functions. Inserting this expression into Eqs. (1) and (2) and by making use of orthogonality of spherical harmonics, the photoionization cross section can be rewritten in the form

$$\sigma(\alpha_0 J_0 \rightarrow \alpha_a J_a M_a, \epsilon) = \frac{4\pi^2\alpha}{2\omega(2J_0+1)} \times \sum_{M_0 \lambda} \sum_{\kappa m_j} \sum_{J J' M} \langle J_a M_a j m_j | J M \rangle \langle J_a M_a j m_j | J' M \rangle \times \left\langle (\alpha_a J_a, \epsilon j l) J M \left| \sum_{i=1}^{N} \boldsymbol{\alpha}_i \mathbf{u}_\lambda e^{i\boldsymbol{k}\cdot\boldsymbol{r}_i} \right| \alpha_0 J_0 M_0 \right\rangle \times \left\langle (\alpha_a J_a, \epsilon j l) J' M \left| \sum_{i=1}^{N} \boldsymbol{\alpha}_i \mathbf{u}_\lambda e^{i\boldsymbol{k}\cdot\boldsymbol{r}_i} \right| \alpha_0 J_0 M_0 \right\rangle^*, \quad (5)$$

where the integration over the electron direction leads to an *incoherent* summation over the electron partial waves with different κ's.

The matrix elements in the last two lines of expression (5) still contain the transition operators $\hat{\mathcal{R}}_\lambda(\boldsymbol{k}) = \sum_{i=1}^{N} \boldsymbol{\alpha}_i \mathbf{u}_\lambda e^{i\boldsymbol{k}\cdot\boldsymbol{r}_i}$ which describes the (relativistic) electron-photon interaction. In other expansions, therefore, we have to decompose this operator into the *multipole* components to allow a further simplification of partial photoionization cross sections. Again, the decomposition of the photon plane waves in $\hat{\mathcal{R}}_\lambda(\boldsymbol{k})$ depends on the particular choice of quantization axis and reads—by using a quantization along the photon momentum—as [28]

$$\mathbf{u}_\lambda e^{i\boldsymbol{k}\cdot\boldsymbol{r}} = \sqrt{2\pi} \sum_{L} \sum_{\pi=0,1} i^L \sqrt{2L+1} (i\lambda)^\pi \mathbf{A}^{\pi}_{L\lambda}, \tag{6}$$

where we introduce the notations $\mathbf{A}^{(e)}_{L\lambda} \equiv \mathbf{A}^{\pi=1}_{L\lambda}$ for the electric and $\mathbf{A}^{(m)}_{L\lambda} \equiv \mathbf{A}^{\pi=0}_{L\lambda}$ for the magnetic multipole fields.

Inserting the decomposition (6) for the photon wave into Eq. (2) and interchanging the sequence of summation ($LM\pi \leftrightarrow i$), we obtain the final expression for the partial photoionization cross section:

$$\begin{aligned}
&\sigma(\alpha_0 J_0 \rightarrow \alpha_a J_a M_a, \boldsymbol{\epsilon}) \\
&\quad = \frac{8\pi^3 \alpha}{2\omega(2J_0+1)} \sum_{t\lambda} \sum_{\kappa} \sum_{JJ'} \sum_{L\pi L'\pi'} i^{L-L'} (i\lambda)^\pi (-i\lambda)^{\pi'} \\
&\qquad \times (-1)^{L+L'} \sqrt{(2L+1)(2L'+1)(2J+1)(2J'+1)} \\
&\qquad \times \langle L'\lambda J_a M_a | t, \lambda + M_a \rangle \langle L\lambda J_a M_a | t, \lambda + M_a \rangle \\
&\qquad \times \begin{Bmatrix} j & J' & J_a \\ J & J_0 & L \\ J_a & L' & t \end{Bmatrix} \langle (\alpha_a J_a, \boldsymbol{\epsilon} lj) J \| H_\gamma(\pi L) \| \alpha_0 J_0 \rangle \\
&\qquad \times \langle (\alpha_a J_a, \boldsymbol{\epsilon} lj) J' \| H_\gamma(\pi' L') \| \alpha_0 J_0 \rangle^*,
\end{aligned} \tag{7}$$

where in the last two lines we made use of the Wigner-Eckart theorem and the standard notation

$$\begin{aligned}
&\langle (\alpha_a J_a, \boldsymbol{\epsilon} lj) J' \| H_\gamma(\pi L) \| \alpha_0 J_0 \rangle \\
&\qquad = i^{-l} \mathrm{e}^{i\Delta_\kappa} \left\langle (\alpha_a J_a, \boldsymbol{\epsilon} lj) J' \left\| \sum_{i=1}^{N} \boldsymbol{\alpha}_i \mathbf{u}_\lambda e^{i\boldsymbol{k}\cdot\boldsymbol{r}_i} \right\| \alpha_0 J_0 \right\rangle
\end{aligned} \tag{8}$$

to denote the reduced matrix elements of the multipole fields together with the proper phase for the emitted electron. In fact, the reduced matrix elements (8) are the *building blocks* in order to represent and to discuss the various properties not only of the atomic photoionization but also of its time-reversed process, the radiative capture of a free (or quasifree) electron into a bound state of ions [29].

Equation (7) displays the general form of the partial cross section for the photoionization of a (few-electron) ion to some specific magnetic sublevel $|\alpha_a J_a M_a\rangle$ of the final ion. Obviously, by performing a summation over all these magnetic sublevels and making use of the standard Racah's algebra, we obtain the *total* photoionization cross section

$$\begin{aligned}
&\sigma(\alpha_0 J_0 \rightarrow \alpha_a J_a, \boldsymbol{\epsilon}) \\
&\quad = \sum_{M_a} \sigma(\alpha_0 J_0 \rightarrow \alpha_a J_a M_s, \boldsymbol{\epsilon}) \\
&\quad = \frac{8\pi^3 \alpha}{\omega(2J_0+1)} \sum_{\kappa J} \sum_{L\pi} \langle (\alpha_a J_a, \boldsymbol{\epsilon} lj) J \| H_\gamma(\pi L) \| \alpha_0 J_0 \rangle,
\end{aligned} \tag{9}$$

which is well known from the literature [29].

B. Polarization of the characteristic radiation

While, of course, Eqs. (7) and (9) can be applied to *all* ions (or atoms) independent of their initial $|\alpha_0 J_0\rangle$ and final $|\alpha_a J_a\rangle$ shell structure, here we consider the particular case of inner-shell photoionization. In such a process, the final ion appears to be in the *excited* state for which the *relative population* of the magnetic sublevels $|\alpha_a J_a M_a\rangle$ following photoionization is described by the partial cross sections (7). Since, however, the direction $\boldsymbol{k}$ of the incident photons is fixed and well defined, this—residual—population is likely to deviate from a statistical distribution. If, moreover, the sublevels with the same modulus of magnetic quantum numbers $|M_a|$ will be equally populated, the ion is said to be *aligned*. The subsequent (radiative) decay of such an—aligned—ion may lead both to an anisotropic angular distribution and to a nonzero *linear polarization* of the characteristic radiation. As usual, here the linear polarization of light is defined in terms of the Stokes parameter [5,14]:

$$\eta_3(\theta) = \frac{I_\parallel(\theta) - I_\perp(\theta)}{I_\parallel(\theta) + I_\perp(\theta)}, \tag{10}$$

where $I_\parallel$ and $I_\perp$ are the intensities of radiation with a polarization vector parallel and perpendicular to the plane formed by the directions of the incident photon beam and emitted characteristic photons and where θ is the angle between these two particular directions.

Beside the population of the excited sublevels (7) and the emission angle θ, the linear polarization (10) of the characteristic x-ray photons depends, of course, on the angular momenta of the initial excited $|\alpha_a J_a\rangle$ and the final ground $|\alpha_b J_b\rangle$ ion states as well as on the *type* of photon transition. For instance, while the linear polarization of the *electric dipole* photons which are emitted in the $J_a = 1 \rightarrow J_b = 0$ decay is given by the well-known expression [14]

$$\eta_3^{(E1)}(\theta) = \frac{(\sigma_0 - \sigma_1)\sin^2\theta}{\sigma_0 \sin^2\theta + \sigma_1(1+\cos^2\theta)}, \tag{11}$$

the Stokes parameter (10) for the *magnetic quadrupole* $J_a = 2 \rightarrow J_b = 0$ transition reads as

$$\eta_3^{(M2)}(\theta) = -\frac{3\sigma_0 \sin^2\theta\cos^2\theta + \sigma_1(1-4\cos^2\theta)\sin^2\theta - \sigma_2 \sin^4\theta}{3\sigma_0 \sin^2\theta\cos^2\theta + \sigma_1(1-3\cos^2\theta+4\cos^4\theta) + \sigma_2(1-4\cos^4\theta)}, \tag{12}$$

where we have introduced the notation $\sigma_{M_a} \equiv \sigma(\alpha_0 J_0 \rightarrow \alpha_a J_a M_a, \epsilon)$ for the partial photoionization cross sections.

As seen from Eqs. (11) and (12) for the electric dipole and magnetic quadrupole transitions, the degree of linear polarization vanishes for the forward ($\theta = 0^\circ$) and backward ($\theta = 180^\circ$) emission angles and is maximal in the direction perpendicular to the incoming photon beam ($\theta = 90^\circ$). In practice, therefore, the linear polarization of the x-ray photon emission is usually measured in this—perpendicular—direction for which the Stokes parameters η_3 can be simplified to [5,14]

$$P_L^{(E1)} \equiv \eta_3^{(E1)}(\theta = 90^\circ) = \frac{\sigma_0 - \sigma_1}{\sigma_0 + \sigma_1} \tag{13}$$

for the $J_a = 1 \rightarrow J_b = 0$ electric dipole transition and to

$$P_L^{(M2)} \equiv \eta_3^{(M2)}(\theta = 90^\circ) = \frac{\sigma_2 - \sigma_1}{\sigma_2 + \sigma_1} \tag{14}$$

for the $J_a = 2 \rightarrow J_b = 0$ magnetic quadrupole decay. In the next two sections, these Stokes parameters are calculated for the $2p^5 3s \rightarrow 2p^6$ radiative decays following inner-shell photoionization of the sodiumlike iron F^{15+} and uranium U^{81+} ions.

III. COMPUTATIONS

As seen from Eqs. (13) and (14), the computation of the linear polarization of the characteristic photon emission can be traced back to the reduced matrix elements (8) which describe the interaction of an ionic bound state with the one-electron continuum due to the presence of the radiation field. In our computations below, these matrix elements have been evaluated by means of the MCDF approach. Within such an approach, both the initial and final bound-ionic states with angular momentum and parity (J^P) are approximated by a linear combination of the so-called configuration-state functions (CSF's) of the same symmetry:

$$\psi_\alpha(PJM) = \sum_{r=1}^{n_c} c_r(\alpha) |\gamma_r PJM\rangle, \tag{15}$$

where n_c is the number of CSF's and $\{c_r(\alpha)\}$ denotes the representation of the atomic state in this basis. In most standard computations, the CSF's are constructed as antisymmetrized products of a common set of orthonormal orbitals and are optimized on the basis of the Dirac-Coulomb Hamiltonian. Further relativistic contributions to the representation $\{c_r(\alpha)\}$ of the atomic states are then added, owing to the given requirements, by diagonalizing the Dirac-Coulomb-Breit Hamiltonian matrix in first-order perturbation theory. For multiple and highly charged ions, moreover, an estimate of the dominant QED contributions (i.e., the self-energy and vacuum polarization of the electronic cloud) is taken into account also by using data from the hydrogenlike ions and a proper scaling of the charge distribution near and around the nucleus. In order to support a reliable estimate of the photoionization amplitudes, a new component (PHOTO) has been developed recently within the framework of the RATIP package [30] which now facilitates the computation of angular distributions and cross sections in a distorted-wave approximation.

IV. RESULTS AND DISCUSSION

A. Fe^{15+} target ion

Over the last two decades, the sodiumlike Fe^{15+} ion has played an important role in astrophysical and laboratory plasma studies as well as in the physics of atomic collisions [31]. For instance, a large number of experimental [32,33] and theoretical [34–36] works have been performed to explore the different—direct and indirect—ionization processes in *electron-impact* ionization of these ions. In contrast to the electron-impact processes, however, much less attention has been previously paid to the *photoionization* of the Fe^{15+} ions, including the case studies of inner-shell vacancy production.

In this contribution, we make use of Eqs. (7) and (8) in order to investigate the ionization of the $2p$ electron of the (initially) sodiumlike Fe^{15+} ($1s^2 2s^2 2p^6 3s$) ion by the incoming unpolarized light. Special attention has been paid, in particular, to the partial cross sections for the photoionization to the individual magnetic sublevels $|2p^5 3s J_a M_a\rangle$ of the residual neonlike ion Fe^{16+} which are required for the analysis of the subsequent radiative decay [cf. Eqs. (13) and (14)]. In Table I, these partial as well as the total cross sections (9) are presented for all four $2p^5 3s\ ^3p_2$, $2p^5 3s\ ^1p_1$, and $2p^5 3s\ ^3p_{0,1}$ excited states and for incoming photon energies in the range $1.25 \leqslant \hbar\omega \leqslant 13.25$ keV. For these energies, the photoionization of the $2p^5 3s\ ^3p_2$ and $2p^5 3s\ ^1p_1$ levels leads to the preferred population of the substates with maximal magnetic quantum numbers ($M_a = \pm 1$ for two $2p^5 3s\ ^1p_1$ levels and $M_a = \pm 2$ for the level $2p^5 3s\ ^3p_2$), indicating an *alignment* along the incoming photon beam direction. A similar alignment of the $2p^5 3s J_a = 1, 2$ excited states has been recently predicted for the electron-impact ionization of sodiumlike Se^{24+} ions [37]. However, while for the electron-impact ionization the ratio $\sigma_{M_a=0}/\sigma_{M_a=J_a}$ of the population cross sections to the substates with the minimum $M_a = 0$ and maximum $M_a = J_a$ magnetic quantum numbers was found not to exceed 1.05, the greater differences in the sublevel population and, hence, the stronger alignment arise due to the photoionization process. As seen from Table I, for example, the cross section ratio $\sigma_{M_a=2}/\sigma_{M_a=0}$ for photoionization to the substates $2p^5 3s\ ^3p_2 M_a = 2$ and $2p^5 3s\ ^3p_2 M_a = 0$ takes the value of 1.14 for near-threshold ionization and increases to

TABLE I. Partial cross sections (in barns) for the photoionization of sodiumlike Fe^{15+} ions initially in their ground state to the magnetic sublevels M_a of the different $2p^5 3s$ excited states of the residual Fe^{16+} ions. The cross sections have been calculated within the electric-dipole approximation (first entries) as well as the exact relativistic theory (second entries) which includes the summation over all multipoles in the electron-photon interaction (6). Apart from the partial cross sections, the total photoionization cross sections (9) are also presented and marked by Σ. Moreover, $x[y]$ denotes $x \times 10^y$.

			$\hbar\omega$ (keV)						
Excited level	M_a	I (keV)	1.25	3.25	5.25	7.25	9.25	11.25	13.25
$2p^5 3s\ ^3P_2$ or	0	1.213	2.85[+4]	1.74[+3]	3.68[+2]	1.23[+2]	5.25[+1]	2.61[+1]	1.44[+1]
$(2p_{1/2}^2 2p_{3/2}^3 3s)_2$			2.86[+4]	1.76[+3]	3.78[+2]	1.28[+2]	5.52[+1]	2.78[+1]	1.55[+1]
	1		2.96[+4]	1.82[+3]	3.85[+2]	1.29[+2]	5.52[+1]	2.75[+1]	1.52[+1]
			2.96[+4]	1.84[+3]	3.94[+2]	1.34[+2]	5.78[+1]	2.91[+1]	1.63[+1]
	2		3.25[+4]	2.03[+3]	4.35[+2]	1.47[+2]	6.33[+1]	3.17[+1]	1.76[+1]
			3.26[+4]	2.06[+3]	4.44[+2]	1.51[+2]	6.57[+1]	3.32[+1]	1.86[+1]
	Σ		1.53[+5]	9.45[+3]	2.01[+3]	6.75[+2]	2.89[+2]	1.44[+2]	8.00[+1]
			1.53[+5]	9.56[+4]	2.05[+3]	6.98[+2]	3.02[+2]	1.52[+2]	8.53[+1]
$2p^5 3s\ ^1P_1$ or	0	1.215	2.79[+4]	1.70[+3]	3.58[+2]	1.19[+2]	5.08[+1]	2.52[+1]	1.39[+1]
$(2p_{1/2}^2 2p_{3/2}^3 3s)_1$			2.80[+4]	1.73[+3]	3.68[+2]	1.24[+2]	5.37[+1]	2.71[+1]	1.51[+1]
	1		3.19[+4]	1.99[+3]	4.24[+2]	1.43[+2]	6.15[+1]	3.08[+1]	1.71[+1]
			3.19[+4]	2.01[+3]	4.33[+2]	1.47[+2]	6.39[+1]	3.23[+1]	1.81[+1]
	Σ		9.16[+4]	5.67[+3]	1.21[+3]	4.05[+2]	1.74[+2]	8.68[+1]	4.81[+1]
			9.18[+4]	5.74[+3]	1.23[+3]	4.19[+2]	1.81[+2]	9.16[+1]	5.13[+1]
$2p^5 3s\ ^3P_0$ or	0	1.226	3.14[+4]	1.99[+3]	4.27[+2]	1.45[+2]	6.24[+1]	3.14[+1]	1.75[+1]
$(2p_{1/2} 2p_{3/2}^4 3s)_0$			3.15[+4]	2.01[+3]	4.36[+2]	1.49[+2]	6.52[+1]	3.31[+1]	1.86[+1]
$2p^5 3s\ ^3P_1$ or	0	1.227	3.21[+4]	2.03[+3]	4.38[+2]	1.49[+2]	6.42[+1]	3.22[+1]	1.79[+1]
$(2p_{1/2} 2p_{3/2}^4 3s)_1$			3.21[+4]	2.06[+3]	4.47[+2]	1.53[+2]	6.67[+1]	3.39[+1]	1.91[+1]
	1		3.11[+4]	1.96[+3]	4.21[+2]	1.43[+2]	6.15[+1]	3.09[+1]	1.72[+1]
			3.12[+4]	1.99[+3]	4.31[+2]	1.48[+2]	6.44[+1]	3.27[+1]	1.84[+1]
	Σ		9.42[+4]	5.96[+3]	1.28[+3]	4.33[+2]	1.87[+2]	9.39[+1]	5.23[+1]
			9.44[+4]	6.03[+3]	1.31[+3]	4.48[+2]	1.96[+2]	9.92[+2]	5.59[+1]

almost 1.22 for photon energy $\hbar\omega = 13.25$ keV.

Apart from the energy dependence of the magnetic sublevel population, we have also explored the effects which arise from the higher (*nondipole*) multipoles in the expansion (6) of the electron-photon interaction. To this end, partial photoionization cross sections have been calculated within both the exact relativistic theory (second entries in Table I) which includes the summation over all multipoles in Eq. (7), and the electric dipole approximation (first entries) obtained by restricting the summation to $L = L' = 1$ and $\pi = \pi' = 1$, respectively. While for near-threshold photoionization both approximations yield basically identical results, they start to differ for higher photon energies where the nondipole contributions result in an enhancement of the cross sections. The strongest nondipole effect arises, of course, for the highest photon energy $\hbar\omega = 13.25$ keV for which the photoionization cross sections are increased by almost 7% if the higher multipoles are taken into account (cf. Table I).

As seen from Eqs. (13) and (14), the partial cross sections for the photoionization to the excited $2p^5 3s$ ion states can be directly used in order to derive the polarization of the subsequent decay photons. In Fig. 1, for example, the degree of linear polarization $P_L^{E1,M2}$ is shown as a function of the incident photon energy for the $2p^5 3s\ ^3p_1 \rightarrow 2p^6\ ^1S_0$ (left panel), $2p^5 3s\ ^1p_1 \rightarrow 2p^6\ ^1S_0$ (middle panel), and $2p^5 3s\ ^3p_2 \rightarrow 2p^6\ ^1S_0$ (left panel) radiative decays. For these three lines, which are usually denoted in atomic spectroscopy as $3F$, $3G$, and $3H$, respectively, the results are presented for both the electric-dipole (--) and the exact relativistic (—) approximations for the partial photoionization cross sections (7). As seen from the figure, the higher-multipole effects in the inner-shell photoionization of sodiumlike Fe^{15+} ions typically reduce the alignment of the excited $2p^5 3s$ states and, hence, the degree of polarization of the characteristic radiation. As usual, these nondipole effects become more pronounced for higher photon energies, where they decrease the polarization parameters $P_L^{E1,M2}$ from 2.23% to 1.70%, from −10.27% to −8.62% and from 7.29% to 6.53% for the $3F$, $3G$, and $3H$ lines, respectively. For the near-threshold ionization, in contrast, the electric dipole approximation gives a reasonable estimation for the degree of linear polarization, the module of which does not exceed, however, 6.5% for all three lines.

B. U^{81+} target ion

As discussed in the previous section, the higher-order contributions to the inner-shell photoionization may strongly affect the polarization of the subsequently emitted photons.

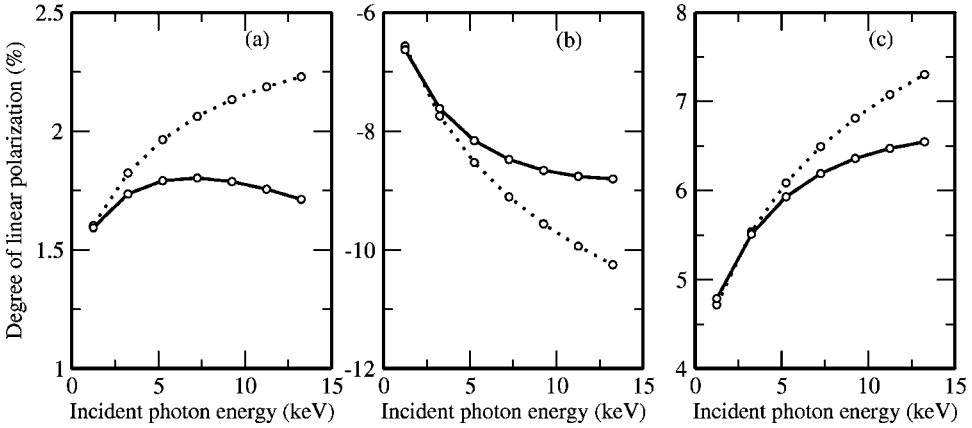

FIG. 1. Degree of linear polarization of the characteristic $2p^5 3s\ ^3p_1 \rightarrow 2p^6\ ^1S_0$ (a), $2p^5 3s\ ^1p_1 \rightarrow 2p^6\ ^1S_0$ (b), and $2p^5 3s\ ^3p_2 \rightarrow 2p^6\ ^1S_0$ (c) x-ray lines following the inner-shell photoionization of the sodiumlike Fe^{15+} ions. Results are presented for the exact relativistic theory (solid lines) as well as the relativistic dipole approach (dashed lines) for the emission of the decay photons perpendicular to the incoming beam direction.

However, while almost 30% depolarization was found for the ionization of sodiumlike Fe^{15+}, even stronger nondipole effects are expected for the *high-Z* domain. To explore these effects, computations were performed for the inner-shell ionization of the sodiumlike uranium ions U^{81+} by photons with energies in the range $I_{2p_{3/2}} \leqslant \hbar\omega \leqslant 1.5 \times I_{2p_{3/2}}$ where $I_{2p_{3/2}} \cong 25$ keV is the $2p_{3/2}$ ionization threshold. Similar to before, special attention was paid to study the population of the $2p^5 3s\ ^3p_2$, $2p^5 3s\ ^1p_1$, and $2p^5 3s\ ^3p_{0,1}$ excited states as obtained within both the electric-dipole approximation and exact relativistic theory which includes the complete summation over the higher multipoles in the electron-photon interaction (6). In contrast to Fe^{15+}, such nondipole effects appear to be more significant for the near-threshold photoionization of the U^{81+} target ions. For example, as seen from Table II, the incorporation of higher multipoles beyond the electric-dipole approximation contributes even for the lowest photon energy of $\hbar\omega = 25.05$ keV to almost 6% for the total ionization cross sections (9).

Beside the total, the partial photoionization cross sections and, hence, the alignment of the excited ion states are also affected by the nondipole effects. Again, in order to study

TABLE II. Partial cross sections (in barns) for the photoionization of sodium like U^{81+} ions initially in their ground state to the magnetic sublevels M_a of the different $2p^5 3s$ excited states of the residual U^{82+} ions. See Table I for further details.

			$\hbar\omega$ (keV)						
Excited level	M_a	I (keV)	25.05	27.05	29.05	31.05	33.05	35.05	37.05
$2p^5 3s\ ^3P_2$ or	0	25.026	9.44[+2]	7.47[+2]	5.99[+2]	4.87[+2]	3.99[+2]	3.31[+2]	2.77[+2]
$(2p_{1/2}^2 2p_{3/2}^3 3s)_2$			9.86[+2]	7.89[+2]	6.41[+2]	5.27[+2]	4.38[+2]	3.68[+2]	3.12[+2]
	1		9.86[+2]	7.81[+2]	6.28[+2]	5.10[+2]	4.19[+2]	3.48[+2]	2.92[+2]
			1.04[+3]	8.29[+2]	6.74[+2]	5.54[+2]	4.61[+2]	3.87[+2]	3.28[+2]
	2		1.12[+3]	8.85[+2]	7.13[+2]	5.82[+2]	4.79[+2]	3.99[+2]	3.36[+2]
			1.19[+3]	9.50[+2]	7.72[+2]	6.35[+2]	5.28[+2]	4.44[+2]	3.76[+2]
	Σ		5.15[+3]	4.08[+3]	3.28[+3]	2.67[+3]	2.20[+3]	1.83[+3]	1.53[+3]
			5.43[+3]	4.35[+3]	3.53[+3]	2.91[+3]	2.42[+3]	2.03[+3]	1.72[+3]
$2p^5 3s\ ^1P_1$ or	0	25.038	9.44[+2]	7.46[+2]	5.98[+2]	4.86[+2]	3.99[+2]	3.31[+2]	2.77[+2]
$(2p_{1/2}^2 2p_{3/2}^3 3s)_1$			9.86[+2]	7.89[+2]	6.41[+2]	5.27[+2]	4.38[+2]	3.68[+2]	3.12[+2]
	1		1.07[+3]	8.51[+2]	6.84[+2]	5.58[+2]	4.60[+2]	3.82[+2]	3.21[+2]
			1.14[+3]	9.10[+2]	7.39[+2]	6.08[+2]	5.06[+2]	4.35[+2]	3.60[+2]
	Σ		3.09[+3]	2.45[+3]	1.97[+3]	1.60[+3]	1.32[+3]	1.09[+3]	9.20[+2]
			3.26[+3]	2.61[+3]	2.12[+3]	1.74[+3]	1.45[+3]	1.22[+3]	1.03[+3]
$2p^5 3s\ ^3P_0$ or	0	28.935	—	—	1.09[+3]	9.06[+2]	7.63[+2]	6.47[+2]	5.54[+2]
$(2p_{1/2} 2p_{3/2}^4 3s)_0$			—	—	1.14[+3]	9.55[+2]	8.10[+2]	6.94[+2]	5.98[+2]
$2p^5 3s\ ^3P_1$ or	0	28.938	—	—	1.09[+3]	9.06[+2]	7.63[+2]	6.48[+2]	5.54[+2]
$(2p_{1/2} 2p_{3/2}^4 3s)_1$			—	—	1.14[+3]	9.55[+2]	8.11[+2]	6.94[+2]	5.98[+2]
	1		—	—	1.08[+3]	9.06[+2]	7.62[+2]	6.47[+2]	5.53[+2]
			—	—	1.14[+3]	9.55[+2]	8.10[+2]	6.93[+2]	5.97[+2]
	Σ		—	—	3.26[+3]	2.72[+3]	2.29[+3]	1.92[+3]	1.66[+3]
			—	—	3.41[+3]	2.86[+3]	2.43[+3]	2.08[+3]	1.79[+3]

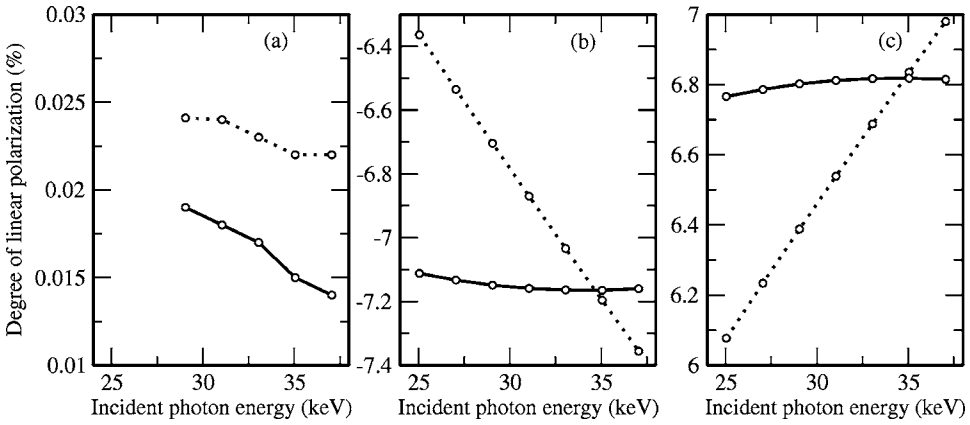

FIG. 2. Degree of linear polarization of the characteristic $2p^5 3s\ ^3p_1 \rightarrow 2p^6\ ^1S_0$ (a), $2p^5 3s\ ^1p_1 \rightarrow 2p^6\ ^1S_0$ (b), and $2p^5 3s\ ^3p_2 \rightarrow 2p^6\ ^1S_0$ (c) x-ray lines following the inner-shell photoionization of the sodiumlike U^{81+} ions. See Table I for further details.

these effects it is more convenient to calculate the linear polarization of the decay radiation which is directly related to the magnetic sublevel population following the ionization process. Figure 2 displays, for example, the Stokes parameters $P_L^{E1,M2}$ of the $3F$, $3G$, and $3H$ characteristic lines in neonlike uranium U^{82+} as a function of the incident photon energy. As seen from the figure, these parameters are negative for the $3G$ dipole transition and positive for the $3F$ and $3H$ lines, indicating the (relatively) small alignment of the excited ion states [cf. Eqs. (13) and (14)]. Similar to the Fe^{15+} case, moreover, this alignment and, hence, the degree of linear polarization are strongly affected by the higher-multipole contributions to the photoionization cross sections (7). As seen from Fig. 2, the nondipole effects are most pronounced for the $3G$ and $3H$ transitions, where the strong enhancement of the linear polarization is observed for the near-threshold ionization. In the particular case of the photon energy $\hbar\omega = 25.05$ keV, for example, the higher multipoles lead to an increase (of the module) of the Stokes parameter P_L from 6.36% to 7.12% for the $3G$ line and from 6.07% to 6.77% for the $3H$ line.

V. SUMMARY AND OUTLOOK

In this work, the inner-shell photoionization of medium- and high-Z, many-electron ions and their subsequent radiative decay have been studied within Dirac's relativistic approach by accounting for the full multipole expansion of the electron-photon interaction. In particular, the general expressions for the *partial* (ionization) cross sections have been derived and used in order to analyze the linear polarization of the characteristic x-ray photons. While, of course, these expressions can be applied to all many-electron ions, independent of their shell structure, detailed computations have been carried out for the $2p$ photoionization of the sodiumlike iron Fe^{15+} and uranium U^{81+} ions and the subsequent $2p^5 3s\ ^3p_2 \rightarrow 2p^6\ ^1S_0$, $2p^5 3s\ ^1p_1 \rightarrow 2p^6\ ^1S_0$, and $2p^5 3s\ ^3p_1 \rightarrow 2p^6\ ^1S_0$ decays. For these three lines, the degree of linear polarization was found to be in the range $|P_L^{E1,M2}| \leqslant 7.2\%$ for the near-threshold ionization and to decrease if the incoming photon energy becomes larger.

Beside the energy dependence, we have also explored how the nondipole effects in the inner-shell photoionization affect the linear polarization of the subsequently emitted photons. From the comparison of our calculations, based on the electric-dipole approximation and the fully relativistic theory, we found that the higher multipoles of the radiation field typically lead to an *enhancement* of the linear polarization of light following ionization of the uranium U^{81+} ions and to its *reduction* for the case of iron Fe^{15+} ions. The most pronounced depolarization effect for the Fe^{15+} ions appeared for the $2p^5 3s\ ^3p_1 \rightarrow 2p^6\ ^1S_0$ decay where the Stokes parameter P_L^{E1} decreases by more than 30% if the nondipole terms in the photoionization cross sections are taken into account.

Another depolarization effect on the characteristic x-ray radiation is expected to arise due to the cascade feeding from the higher-lying levels to the magnetic sublevel population of the excited $2p^5 3s$ ion states. The detailed analysis of such cascade contributions which are not included in the present calculations is currently underway and will be presented in a forthcoming paper.

ACKNOWLEDGMENTS

This work has been supported by the BMBF and GSI under Project No. KS-FRT. One of the authors (M.K.I.) gratefully acknowledges financial support from the DFG Schwerpunktprogram 1145 for his short-term visit to Kassel University during May 2004.

[1] S. Flügge, W. Mehlhorn, and V. Schmidt, Phys. Rev. Lett. **29**, 7 (1972).

[2] U. Fano and J. H. Macek, Rev. Mod. Phys. **45**, 553 (1973).

[3] E. G. Berezhko, N. M. Kabachnik, and V. S. Rostovsky, J. Phys. B **11**, 1749 (1977).

[4] K. Blum, *Density Matrix Theory and Applications* (Plenum, New York, 1981).

[5] E. G. Berezhko and N. M. Kabachnik, J. Phys. B **10**, 2467

(1977).
[6] K. J. Reed and M. H. Chen, Phys. Rev. A **48**, 3644 (1993).
[7] E. Haug, Sol. Phys. **61**, 129 (1979); Sol. Phys. **71**, 77 (1981).
[8] E. Källne and J. Källne, Phys. Scr. **T17**, 152 (1987).
[9] J. C. Kieffer, J. P. Matte, M. Chaker, Y. Beaudoin, C. Y. Chien, S. Coe, G. Mourou, J. Dubau, and M. K. Inal, Phys. Rev. E **48**, 4648 (1993).
[10] J.-C. Hénoux and E. Vogt, Phys. Scr. **T78**, 60 (1998).
[11] P. Beiersdorfer, J. Crespo López-Urrutia, V. Decaux, K. Widmann, and P. Neill, Rev. Sci. Instrum. **68**, 1073 (1997).
[12] P. Beiersdorfer, G. Brown, S. Utter, P. Neill, K. J. Reed, A. J. Smith, and R. S. Thoe, Phys. Rev. A **60**, 4156 (1999).
[13] D. L. Robbins, A. Ya. Faenov, T. A. Pikuz, H. Chen, P. Beiersdorfer, M. J. May, J. Dunn, K. J. Reed, and A. J. Smith, Phys. Rev. A **70**, 022715 (2004).
[14] M. K. Inal and J. Dubau, J. Phys. B **20**, 4221 (1987).
[15] H. L. Zhang, D. H. Sampson, and R. E. H. Clark, Phys. Rev. A **41**, 198 (1990).
[16] M. H. Chen and J. H. Scofield, Phys. Rev. A **52**, 2057 (1995).
[17] C. J. Fontes, H. L. Zhang, and D. H. Sampson, Phys. Rev. A **59**, 295 (1999).
[18] G. J. Ferland, Annu. Rev. Astron. Astrophys. **41**, 517 (2003).
[19] W. R. Alling and W. R. Johnson, Phys. Rev. **139**, A1050 (1965).
[20] R. H. Pratt, A. Ron, and H. K. Tseng, Rev. Mod. Phys. **45**, 273 (1973).
[21] H. K. Tseng, R. H. Pratt, S. Yu, and A. Ron, Phys. Rev. A **17**, 1061 (1977).
[22] K. N. Huang, Phys. Rev. A **22**, 223 (1980).
[23] J. H. Scofield, Phys. Rev. A **40**, 3054 (1989).
[24] A. N. Grum-Grzhimailo, J. Phys. B **34**, L359 (2001).
[25] N. A. Cherepkov and S. K. Semenov, J. Phys. B **34**, L211 (2001).
[26] A. Surzhykov, S. Fritzsche, and Th. Stöhlker, Phys. Lett. A **289**, 213 (2001).
[27] J. Eichler and W. Meyerhof, *Relativistic Atomic Collisions* (Academic Press, San Diego, 1995).
[28] M. E. Rose, *Elementary Theory of Angular Momentum* (Wiley, New York, 1953).
[29] S. Fritzsche, A. Surzhykov, and Th. Stöhlker, Phys. Rev. A **72**, 012704 (2005).
[30] S. Fritzsche, J. Electron Spectrosc. Relat. Phenom. **114–16**, 1155 (2001).
[31] A. Müller, Comments At. Mol. Phys. **27**, 1 (1991).
[32] D. C. Gregory, L. J. Wang, F. W. Meyer, and K. Rinn, Phys. Rev. A **35**, 3256 (1987).
[33] J. Linkemann, A. Müller, J. Kenntner, D. Habs, D. Schwalm, A. Wolf, N. R. Badnell, and M. S. Pindzola, Phys. Rev. Lett. **74**, 4173 (1995).
[34] K. J. LaGattuta and Y. Hahn, Phys. Rev. A **24**, 2273 (1981).
[35] S. S. Tayal and R. J. W. Henry, Phys. Rev. A **39**, 3890 (1989).
[36] M. H. Chen, K. J. Reed, and D. L. Moores, Phys. Rev. Lett. **64**, 1350 (1990).
[37] H. L. Zhang, D. H. Sampson, and M. K. Inal, Phys. Rev. A **63**, 052713 (2001).